Analytical modeling of deposited filaments for high viscosity material-based piston-driven direct ink writing

Yongqiang Tu, Alaa Hassan, Ali Siadat, Gongliu Yang

Analytical modeling of deposited filaments for high viscosity material in piston-driven direct ink writing

Yongqiang Tu[a,b], Alaa Hassan[c,*], Ali Siadat[b], Gongliu Yang[a]
(*Corresponding author: Yongqiang Tu; E-mail addresses: alaa.hassan@univ-lorraine.fr)
[a]School of Instrumentation and Optoelectronic Engineering, Beihang University, Beijing 100191, PR China
Arts et Métiers ParisTech, LCFC, F-57000 Metz, France
[c]Université de Lorraine, ERPI, F-54000 Nancy, France

Abstract

Piston-driven direct ink writing (DIW) was developed as a promising additive manufacturing technique to fabricate complex parts with high viscosity material and many efforts have been made in analytical modeling for this process. However, the influences of material properties and process parameters on deposition statuses and height of deposited filaments have been poorly characterized. This study provides an analytical model to predict flow rate, deposition statuses, width and height of deposited filaments. To fulfill this objective, firstly, an analytical model of flow rate is described to predict the flow rate in time domain. Secondly, three deposition statuses are summarized and analytical dividing lines are derived to determine deposition statuses depend on the dimensionless nozzle velocity and the dimensionless height. Thirdly, width and height of deposited filaments are modeled and predicted based on the determined deposition statuses. Finally, Nivea Crème is selected as high viscosity material reference and flow rate, filaments deposition experiments are conducted to verify the proposed model. The effectiveness and prediction accuracy of the proposed model is verified as the relative errors between analytical and experimental results of flow rate are less than 4.31% and the relative errors between analytical and experimental results of width and height are less than 3.90%.

Keywords

Analytical modeling; Deposited filaments; High viscosity material; Direct ink writing

1. Introduction

Additive manufacturing (AM) is an advanced manufacturing technology that directly prints three-dimensional (3D) parts by stacking material layer by layer based on a digital 3D computer-aided design (CAD) model [1]. Compared with traditional manufacturing techniques such as forging, casting and machining, AM has the advantages of digitization, material saving, material diversification and the ability to easily manufacture complex parts, which meet the requirements of high precision, structural freedom and customizability for the

development of new materials and new structures in medicine, aviation, aerospace and electronics [2]. According to ISO/ASTM 52900 (2015) [3], AM is divided to seven categories: binder jetting, directed energy deposition, material extrusion, material jetting, powder bed fusion, sheet lamination and vat photo polymerization.

Direct ink writing (DIW) belongs to the material extrusion AM according to the principle. The biggest advantage of DIW is material compatibility, i.e., materials that can be prepared as inks can be processed using DIW [4]. The principle of DIW is to prepare the material in paste or slurry type with good printability called "ink" and extrude the ink from a nozzle into continuous filaments using mechanical force (piston or screw drive) or pneumatic force, and the filaments are deposited into layer-wise 3D parts [5]. For extrusion method, as concluded by [6], screw or pneumatic force driven DIW both have the disadvantage that the flow rate can be significantly affected by fluid flow behavior and air compressibility; and piston-driven DIW is the most promising as the flow rate is dependent only on the piston movement. For ink preparation, there are two strategies as summarized by [7]: the first one utilizes low viscosity inks with assisted-deposition means like ultraviolet (UV)-thermal curing [8], suspended hydrogels [9] or chemical process [10]; the second prepares high viscosity inks with shear-thinning and viscoelastic properties which can be extruded from a nozzle and deposited to a 3D object directly. Low viscosity material DIW needs to introduce additional assisted-deposition systems and has disadvantage of high cost, low processing efficiency and low accuracy. High viscosity materials are development trend for DIW. For example, many scholars have focused on high viscosity material DIW and successfully applied this technique in tissue engineering [11], rubber processing [12], batteries [13], soft robots [14] and sensors [15]. Considering the development trend of DIW, our work has focused on piston-driven DIW with high viscosity material.

In recent years, to understand how the material properties and the process parameters relate to the resolution of printed parts in high viscosity material DIW, analytical modeling of deposited filaments (DF) has been a research interest. Vlasea et al. [16] described an analytical model for line width of DF by simplifying the DF's cross-sectional profile as an elliptical segment. Lee et al. [17] developed a model for DIW to predict the width of DF with an equation describing the DF's area of a half-ellipse. Suntornnond et al. [18] proposed a mathematical model to predict the width of DF by assuming the DF's cross-sectional profile was circular. Haghbin et al. [19] predicted the sizes of DF using three geometric models of rectangle, oblong and ellipse for extrusion-based 3D printing. All these studies established analytical models of the DF by first assuming that the cross sections of DF were constant shapes and the shapes were simplified as circle, half-ellipse, ellipse, rectangle or oblong. However, cross-sectional shapes of DF will change under different conditions of inks and process parameters [20]. Furthermore, few research works have been trying to predict height of DF in analytical model. However, layer height largely affects the roughness, dimensional accuracy and tolerances of the final parts for extrusion-based 3D printing [21]. Therefore, there is a need of further development on how material properties and process parameters affect the shapes of cross section in analytical model prediction; and the model also needs to predict the height of DF.

In this study, an analytical model is created to predict flow rate, deposition statuses, width and height of DF for high viscosity material in piston-driven DIW. The developed model

overcomes the shortcomings of predictions in previous works by analyzing the effect of material properties and process parameters on cross section shapes and adding height prediction. Next, Nivea Crème is selected as high viscosity material reference and experiments were conducted to verify the proposed model.

Nomenclature		d_n	Inner diameter of nozzle
τ	Shear stress	Q_u	Steady-state flow rate under a unit pressure
$\dot{\gamma}$	Shear rate	τ_w	Shear stress at nozzle wall
τ_0	Yield stress	v_e	Average velocity of extruded filament
K	Consistency index	α	Die-swelling factor
n	Flow index	h	Distance between nozzle bottom and substrate
A_p	Cross section area of piston	v_n	Nozzle velocity
D_p	Piston diameter	h_d	Height of deposited filament
v_p	Piston velocity	w_d	Width of deposited filament
Q	Flow rate	θ_C	Static contact angle
L_0	Initial fill length	V^*	Dimensionless nozzle velocity, = v_n / v_e
t	Time since the piston stated moving	H^*	Dimensionless height, = $h / \alpha d_n$
B	Bulk modulus	D_n	Outer diameter of nozzle
P	Pressure in syringe	β	Ratio of D_n to d_n, = D_n / d_n
ρ	Density	γ	$\left(\theta_C - \frac{\sin 2\theta_C}{2}\right)\left(\frac{1}{1-\cos\theta_C}\right)^2$
L_n	Length of nozzle	d_f	Diameter of deposited filament under freeform-deposition
A_n	Inner cross section area of nozzle	λ	$\left(\theta_C - 2\sin 2\theta_C\right)/\pi$

2. Analytical model development

The analytical model development of DF in piston-driven DIW includes three steps: the first step is to model the flow rate of extruded filaments; the second step is to determine deposition statuses of DF based on process parameters; the third step is to establish model of width and height of DF under the determined deposition status.

In the first step, flow rate model proposed by [6] is used directly as the model considers both material properties and process parameters and [16] has verified this model by adopting the model in their work. In the second and third step, the novelty of this work is that the effect of material properties and process parameters on cross section shapes of DF is considered and height is predicted as well as width.

2.1. Flow rate

The flow rate model of extruded filaments in piston-driven DIW presented by [6] was used in this study. The flow rate model described by [6] made the following assumptions.

1) Only material compressibility was considered and flow behavior was neglected in the syringe as fluid velocities in the syringe were small and the pressure in syringe was uniform because the height of fluid level in syringe was short.
2) Material compressibility was neglected and flow behavior was considered in the nozzle as fluid volume in the nozzle was much small;
3) The process was isothermal, material properties were time-independent, the flow was laminar and there was no slip between the fluid and the nozzle wall;
4) Flow behavior of high viscosity material was expressed using Hershel-Bulkley model as shown in Eq. (1) [22].

$$\tau = \tau_0 + K\dot{\gamma}^n \tag{1}$$

where τ (unit: Pa) and $\dot{\gamma}$ (unit: s^{-1}) were shear stress and shear rate; τ_0 (unit: Pa), K (unit: $Pa \cdot s^n$) and n (unit: dimensionless) were rheological properties called as yield stress, consistency index, flow index. τ_0 was the critical value of shear stress to determine whether the ink was flowing, i.e., if stress< τ_0, the material behaved as a rigid solid, otherwise it behaved as a fluid. K measured the viscosity as viscosity was proportional to K. n expressed the flow properties and the n value of the inks used in DIW needed to satisfy 0< n <1 to ensure that the inks were shear-thinning fluids [23]. For certains inks, the values of τ_0, K and n were determined experimentally.

Based on these assumptions, pressure in the syringe and flow rate leaving the nozzle were derived. Eq. (2) was the time domain function of pressure driven by the piston movement and Eq. (3) was the Laplace function of the flow rate driven by the pressure in the syringe.

$$A_p v_p - Q = \frac{A_p\left(L_0 - v_p t\right)}{B} \cdot \frac{dP}{dt} \tag{2}$$

where A_p was the cross section area of the piston and was calculated by $\pi D_p^{\,2}/4$ (D_p was the piston diameter), v_p was the piston velocity, Q was the flow rate, L_0 was the initial fill length in syringe of ink, t was the time since the piston stated moving, B was the bulk modulus of ink, P was the pressure in syringe.

$$\frac{Q(s)}{P(s)} = \frac{Q_u}{s\rho L_n Q_u / A_n + 1} \tag{3}$$

where ρ was the ink density, L_n and A_n were the length and inner cross section area of the nozzle, A_n was calculated by $\pi d_n^{\,2}/4$ (d_n was the inner diameter of nozzle), Q_u was the steady-state flow rate under a unit pressure and was calculated by Eq. (4).

$$Q_u = \frac{\pi d_n^{\,3}}{8PK^{1/n}\tau_w^{\,3}}\left(\tau_w - \tau_0\right)^{\frac{n+1}{n}} \times \left[\frac{n}{3n+1}\tau_w^{\,2} + \frac{2n^2}{(2n+1)(3n+1)}\tau_w\tau_0 + \frac{2n^3}{(n+1)(2n+1)(3n+1)}\tau_0^{\,2}\right] \tag{4}$$

where τ_w was the shear stress at the nozzle wall and was expressed by Eq. (5).

$$\tau_w = \frac{d_n}{4L_n}\left(P + L_n\rho g - 1.12\rho\left(Q / A_n\right)^2\right) \tag{5}$$

Based on the Eq. (2) to Eq. (5) derived by [6], the calculation flowchart of the flow rate model

for extruded filaments was plotted in Fig. 1. The analytical results of flow rate were calculated using Simulink in the software Matlab R2021b (MathWorks, Inc., USA).

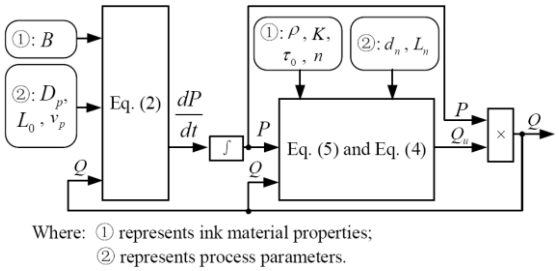

Fig. 1. Calculation flowchart of the flow rate model for extruded filaments.

2.2. Deposition statuses

The deposition process and the process parameters of DIW were illustrated in Fig. 2 (a). Ink was filled in the syringe at the initial filled length L_0 and the full nozzle first. When piston started moving at a fixed velocity v_p, the pressure in the syringe increased and made the τ_w increase. When τ_w exceeded the τ_0, ink started to be extruded out from nozzle. The average velocity of extruded filament was v_e which was calculated by Q / A_n. The diameter of the extruded filament in the air was αd_n where α was the die-swelling factor which described the post-extrusion expansion of the ink and α was determined experimentally [24]. By setting the distance between nozzle bottom and substrate as h and the nozzle velocity related to substrate in the horizontal direction as v_n, the extruded filament was deposited on the substrate.

Through observations of cross section shapes under different process parameters, it was summarized that there were three deposition statuses for cross section shapes of DF: over-deposition, pressed-deposition and freeform-deposition. When h was much smaller than αd_n or v_n was much smaller than v_e, the DF was in over-deposition status. In over-deposition status as shown in Fig. 2 (b), excessive ink was squeezed out beyond the outer diameter of the nozzle and width, height of DF is irregular and cannot be predicted. When h and v_n increased, the status would change to pressed-deposition as shown in Fig. 2 (c) first and then changed to freeform-deposition as shown in Fig. 2 (d). In pressed-deposition status, the height of DF h_d was equal to h as DF was pressed by nozzle bottom and the two ends of the cross section of DF were regular semicircles with a diameter of h_d. In freeform-deposition status, the filament was deposited without nozzle contact and cross section shape was a part of circle dependent on the static contact angle θ_C between the ink and the substrate (θ_C was determined experimentally) [25].

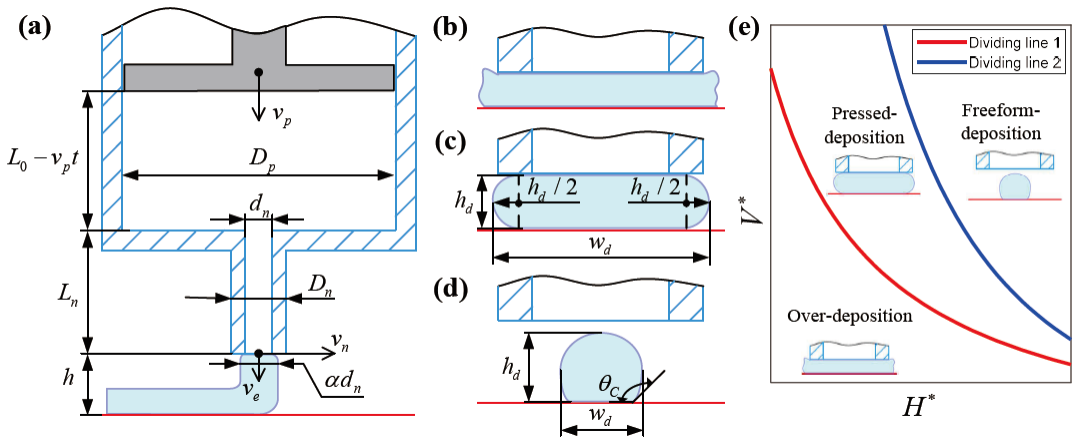

Fig. 2. Analyses of deposition statuses and cross section shapes of DF: (a) illustration of deposition process and process parameters; three deposition statuses for cross section shapes of DF as (b) over-deposition, (c) pressed-deposition and (d) freeform-deposition; (e) cross section shapes statuses division.

To determine deposition statuses, the dimensionless nozzle velocity $V^* = v_n / v_e$ and the dimensionless height $H^* = h / \alpha d_n$ were introduced [26]. Using the law of conservation of mass, the conditions of over-deposition and freeform-deposition could be expressed as Eq. (6) and Eq. (7), respectively.

$$\frac{\pi}{4} d_n^2 v_e \geq h \cdot D_n \cdot v_n \tag{6}$$

$$\frac{\pi}{4} d_n^2 v_e \leq \left(\theta_C - \frac{\sin 2\theta_C}{2}\right)\left(\frac{h}{1-\cos\theta_C}\right)^2 v_n \tag{7}$$

where D_n was the outer diameter of the nozzle.

Then, Eq. (6) and Eq. (7) were simplified as Eq. (8) and Eq. (9), respectively using V^* and H^*.

$$V^* \leq \frac{\pi}{4\alpha\beta} \cdot \frac{1}{H^*} \tag{8}$$

where β was the ratio of D_n to d_n ($\beta = D_n / d_n$).

$$V^* \geq \frac{\pi}{4\alpha^2\gamma} \cdot \left(\frac{1}{H^*}\right)^2 \tag{9}$$

where γ represented $\left(\theta_C - \frac{\sin 2\theta_C}{2}\right)\left(\frac{1}{1-\cos\theta_C}\right)^2$.

The dividing line 1 (solid red line) and dividing line 2 (solid blue line) described by Eq. (8) and Eq. (9) respectively were plotted in Fig. 2 (e) to predict deposition statuses under different V^* and H^*. Combinations of V^* and H^* were divided into three areas by dividing line 1 and dividing line 2: area below dividing line 1 represented over-deposition, area between dividing line 1 and dividing 2 represented pressed-deposition and area above dividing 2 represented freeform-deposition.

2.3. Width and height

After deposition statuses determination, the width and height were modeled and predicted for certain deposition status. Over-deposition status with unstable width of DF led to low printing accuracy and should be avoided. Pressed-deposition and freeform-deposition statuses with controlled width and height were suitable deposition statuses for DIW. Width and height of DF in pressed-deposition and freeform-deposition statuses were modeled, respectively.

Mass conservations of DF in pressed-deposition and freeform-deposition statuses were expressed as Eq. (10) and Eq. (11), respectively.

$$\left.\begin{array}{c} \frac{\pi}{4} d_n^{\,2} v_e = \left(h_d \left(w_d - h_d \right) + \frac{\pi}{4} h_d^{\,2} \right) v_n \\ h_d = h \end{array}\right\} \tag{10}$$

$$\left.\begin{array}{c} \frac{\pi}{4} d_n^{\,2} v_e = \left(\frac{\theta_C}{4} d_f^{\,2} - \frac{\sin 2\theta_C}{2} d_f^{\,2} \right) v_n \\ w_d = \begin{cases} d_f \sin\theta_C, \left(\theta_C \le \pi/2\right) \\ d_f, \left(\theta_C > \pi/2\right) \end{cases} \\ h_d = \frac{d_f}{2}\left(1 - \cos\theta_C\right) \end{array}\right\} \tag{11}$$

where d_f was diameter of DF under freeform-deposition status.

By simplifying Eq. (10), the width and height of DF in pressed-deposition status were modeled in Eq. (12) and Eq. (13).

$$w_d = \frac{\pi d_n}{4\alpha} \cdot \frac{1}{H^*} \cdot \frac{1}{V^*} + \left(1 - \frac{\pi}{4}\right) h \tag{12}$$

$$h_d = h \tag{13}$$

By simplifying Eq. (11), the width and height of DF in freeform-deposition status were modeled in Eq. (14) and Eq. (15).

$$w_d = \begin{cases} d_n \sin\theta_C / \sqrt{V^* \lambda}, \left(\theta_C \le \pi/2\right) \\ d_n / \sqrt{V^* \lambda}, \left(\theta_C > \pi/2\right) \end{cases} \tag{14}$$

$$h_d = d_n \left(1 - \cos\theta_C\right) / \left(2\sqrt{V^* \lambda}\right) \tag{15}$$

where λ represented $\left(\theta_C - 2\sin 2\theta_C\right)/\pi$.

3. Experimental verification

3.1. Material and DIW 3D printer

Nivea Crème Art. No. 80104 (Beiersdorf Global AG, Germany) was selected as high viscosity material to verify the proposed model because Nivea Crème was the printability reference and representative for high viscosity material in ink preparation and process parameters

selection for DIW [27]. Material properties of Nivea Crème were obtained using the results in our previous work [28] and listed in Table 1.

Table 1

Material properties of Nivea Crème.

Description	Parameter	Value
Density	ρ	972 kg/m^3
Bulk modulus	B	3.0x10^9 Pa
Yield stress	τ_0	563 Pa
Consistency index	K	867 $Pa \cdot s^n$
Flow index	n	0.045

A piston-driven DIW 3D printer TM-081 (Tobeca Company, France) was used to conduct experiments of flow rate and filaments deposition. The process parameters related to DIW 3D printer's equipment dimensions were listed in Table 2.

Table 2

Process parameters related to DIW 3D printer's equipment dimensions.

Description	Parameter	Value
Piston diameter	D_p	21.6 mm
Length of nozzle	L_n	18 mm
Inner diameter of nozzle	d_n	0.84 mm
Outer diameter of nozzle	D_n	1.22 mm

3.2. Flow rate

According to mass conversation, in steady flow state, the flow rate can be calculated by Eq. (16) and the relationship between v_p and v_e in steady flow state was expressed as Eq. (17).

$$Q = \frac{\pi}{4} D_p^{\,2} v_p = \frac{\pi}{4} d_n^{\,2} v_e \tag{16}$$

$$v_p = \left(d_n / D_p\right)^2 v_e \tag{17}$$

Flow rate experiments were conducted by controlling the DIW 3D printer to extrude Nivea Crème for 6 minutes under 5 levels of v_p and the 5 levels of v_p were calculated using Eq. (17) by setting the values of v_e from 3 mm/s to 15 mm/s at a fixed interval of 3 mm/s. Flow rates were measured by weighing the material dispensed using an analytical balance ME54 (KERN & SOHN, Germany) with a resolution of 0.1 mg. Each experiment was conducted three times and experimental flow rates were expressed as the mean ± standard deviation.

3.3. Deposition statuses, width and height

DF were produced by controlling V^* and H^* at 2-levels of v_p in the DIW 3D printer with a glass substrate. V^* was varied from 0.4 to 1.6 at a fixed interval of 0.4 and H^* was varied

from 0.3 to 1.8 at a fixed interval of 0.3. 2-levels of v_p were obtained through Eq. (17) by setting the values of v_e as 6 mm/s and 12 mm/s, respectively. Under each setting of process parameters, there 80 mm long filaments were deposited in the steady-state flow stage on the substrate. A camera (Canon LEGRIA HF R86 Noir, Canon Inc., Japan) was used to capture top and side views of DF to determine deposition statuses. In the top view of DF, the width of DF was measured at a fixed sampling interval of 5 mm. In the side view of DF, the height of DF was measured in the end face of three filaments. The average and standard deviation were calculated for 45 sampling points in width measurement and 3 sampling points in height measurement. Experimental width and height were expressed as the mean ± standard deviation.

4. Results and discussion

4.1. Flow rate

Based on the proposed flow rate model described in Section 2.1 and the calculation flowchart (Fig. 1), the analytical flow rates under 5 levels of v_p in time-domain from 0 to 370 s (the extrusion time was 360s) were calculated using Simulink and plotted in Fig. 3 (a). To fully understand the extrusion process, the local enlarged views at the starting time and the end time were plotted in Fig. 3 (b) and Fig. 3 (c), respectively. At the starting time shown in Fig. 3 (b), there was a time delay of extrusion as the pressure in the syringe took time to increase τ_w beyond τ_0 to allow ink in the nozzle to flow. Then, there was an unstable flow from starting flow moment to steady-state flow stage. After time delay and unstable flow at the starting time, the flow rate stayed at a constant value related to v_p in a steady-state flow stage. The time of extrusion delay and unstable flow decreased as v_p increased. At the end time shown in Fig. 3 (c), there was unstable flow after piston stopped moving as the pressure in the syringe took time to decrease. To improve the printing accuracy, extruded filaments at the start and end should be avoided to control filament deposition at the steady-state flow stage.

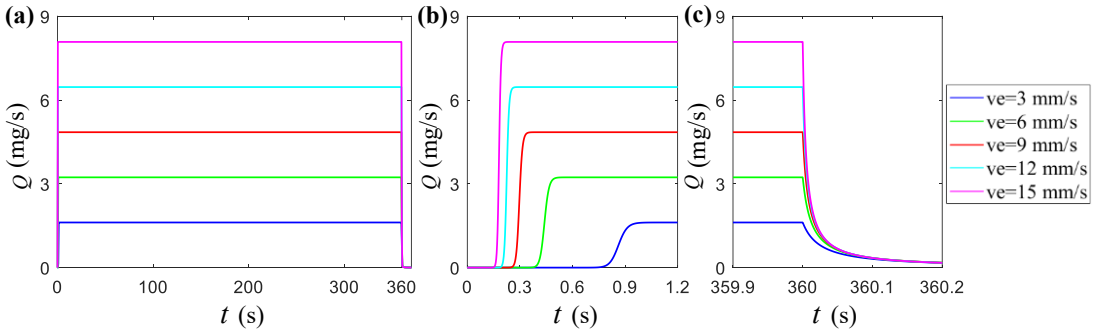

Fig. 3. Analytical results of Flow rate: (a) flow rate in time domain; (b) local enlarged view at the starting time; (c) local enlarged view at the end time.

The analytical model of flow rate was verified as the relative error of analytical and

experimental results for flow rate under 5 levels of v_p was less than 4.31% as shown in Table 3. Analytical flow rate in steady-state flow stage obtained using the described model was exactly same as the analytical flow rate obtained using Eq. (16). Thus, Eq. (16) can be used directly to calculate the flow rate of extruded filaments in steady-state flow stage. However, the described analytical model was necessary to understand the entire extrusion process in time domain because Eq. (16) could only give a constant flow rate value in steady-state flow stage instead of a description for the time-domain extrusion process. According to Eq. (16), in the piston-driven DIW, the flow rate in steady-state flow stage depended only on piston velocity and piston diameter. Material properties of ink and L_0 had no influence on the flow rate.

Table 3

Analytical and experimental results of flow rate.

Setting of v_e (mm/s)	3	6	9	12	15
Analytical flow rate using Eq. (16) (mg/s)	1.62	3.23	4.85	6.46	8.08
Analytical flow rate in steady-state flow stage using the model (mg/s)	1.62	3.23	4.85	6.46	8.08
Experimental flow rate (mg/s)	1.55±0.14	3.09±0.07	4.71±0.07	6.22±0.12	7.90±0.08
Relative error (%)	4.08	4.31	2.78	3.74	2.25

4.2. Deposition statuses, width and height

Values of α and θ_C were measured using the method described by [20]. As shown in Fig. 4 (a), a section of filament was printed in the steady-state coiling regime which ensured the filament was not stretched by the translational motion of the nozzle. As shown in Fig. 4 (b), α was calculated by dividing the cross-section diameter of the filament by the d_n and θ_C was measured directly. As shown in Fig. 4 (c) and Fig. 4 (d), the values of α and θ_C were measured as 1 and π respectively under 5-levels of v_p by setting the value of v_e from 3 mm/s to 15 mm/s at a fixed interval of 3 mm/s. Moreover, the piston velocity had no influence on both the values of α and θ_C.

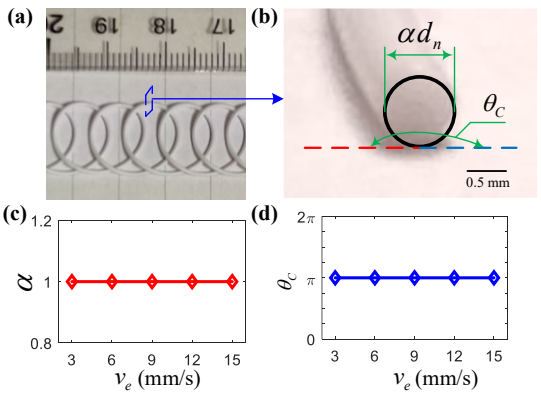

Fig. 4. Measurement of values of α and θ_C: (a) top view of DF; (b) side view of DF; (c) results of

α under 5-levels of piston velocity; (d) results of θ_C under 5-levels of piston velocity.

Process parameters and measured values of α and θ_C were substituted into the proposed models of deposition statuses, width and height to give the analytical statuses division as shown in Fig. 5 and analytical width (Table 4), analytical height (Table 5). Analytical width and height only depended on V^* and H^*. To verify the effectiveness of the proposed model for deposition statuses, width and height, filaments deposition experiments were conducted and then experimental width and height were measured. The experimental deposition statuses by setting the values of v_e as 6 mm/s and 9 mm/s were plotted in Fig. 5 (a) and Fig. 5 (b), respectively. Symbols presented in Fig. 5 were illustrated in Fig. 6. Experimental results of width and height by setting the values of v_e as 6 mm/s were listed in Table 6 and Table 7, respectively. Experimental results of width and height by setting the values of v_e as 9 mm/s were listed in Table 8 and Table 9, respectively. In the Table 6 to Table 9, symbol + represented over-deposition; symbol × represented discontinuous filaments; symbol ▲ represented tortuous filaments.

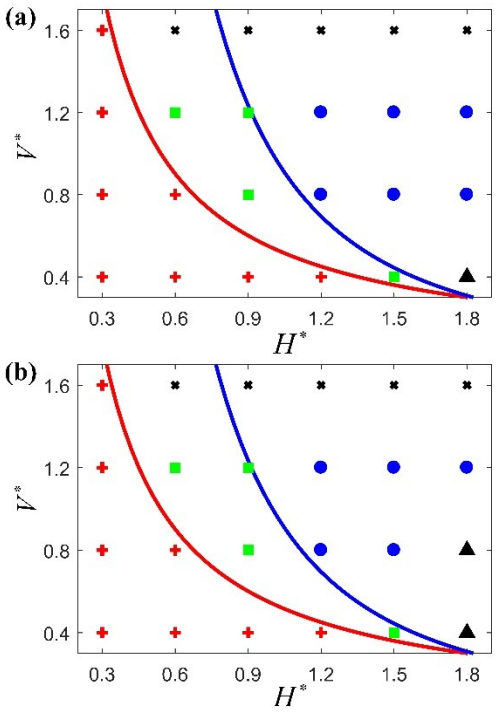

Fig. 5. Analytical and experimental cross section shapes statuses under 2-levels of v_p by setting the values of v_e as (a) 6 mm/s and (b) 9 mm/s.

Symbol	Description	Illustration
	Dividing line 1	Analytical dividing lines obtained by the model
	Dividing line 2	
✚	Experimental over-deposition	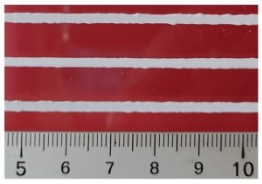 Irregular width and height
■	Experimental pressed-deposition	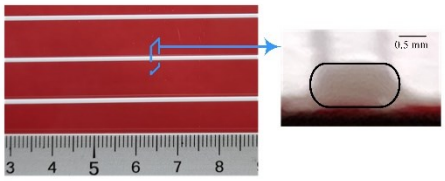
●	Experimental freeform-deposition	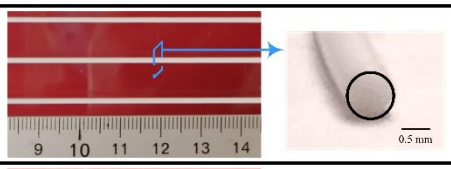
▲	Experimental tortuous filaments	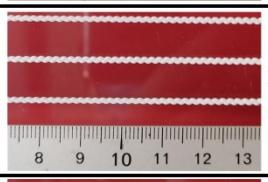 Irregular width and height
✖	Experimental discontinues filaments	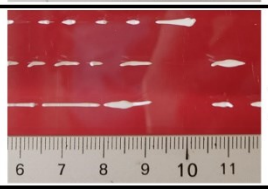 Irregular width and height

Fig. 6. Illustrations of symbols in Fig. 5.

Table 4

Analytical width results (width unit: mm).

V^* \ H^*	0.3	0.6	0.9	1.2	1.5	1.8
0.4	+	0.8	0.66	0.66	0.66	0.66
0.8	+	1.03	0.78	0.77	0.77	0.77
1.2	+	+	1.08	0.94	0.94	0.94
1.6	+	+	+	+	1.38	1.33

Table 5

Analytical height results (height unit: mm).

V^* \ H^*	0.3	0.6	0.9	1.2	1.5	1.8
0.4	+	0.5	0.66	0.66	0.66	0.66
0.8	+	0.5	0.75	0.77	0.77	0.77
1.2	+	+	0.75	0.94	0.94	0.94
1.6	+	+	+	+	1.25	1.33

Table 6

Experimental width results when v_e was set as 6 mm/s (width unit: mm).

V^* \ H^*	0.3	0.6	0.9	1.2	1.5	1.8
0.4	+	×	×	×	×	×
0.8	+	1.00±0.04	0.81±0.03	0.80±0.05	0.79±0.03	0.79±0.04
1.2	+	+	1.10±0.02	0.97±0.03	0.97±0.03	0.97±0.04
1.6	+	+	+	+	1.43±0.05	▲

Table 7

Experimental height results when v_e was set as 6 mm/s (height unit: mm).

V^* \ H^*	0.3	0.6	0.9	1.2	1.5	1.8
0.4	+	×	×	×	×	×
0.8	+	0.5±0.01	0.75±0.01	0.80±0.05	0.79±0.03	0.79±0.04
1.2	+	+	0.75±0.01	0.97±0.03	0.97±0.03	0.97±0.04
1.6	+	+	+	+	1.25±0.02	▲

Table 8

Experimental width results when v_e was set as 9 mm/s (width unit: mm).

V^* \ H^*	0.3	0.6	0.9	1.2	1.5	1.8
0.4	+	×	×	×	×	×
0.8	+	1.07±0.06	0.79±0.03	0.77±0.03	0.77±0.03	0.77±0.05
1.2	+	+	1.06±0.04	0.95±0.04	0.95±0.03	▲
1.6	+	+	+	+	1.35±0.04	▲

Table 9

Experimental height results when v_e was set as 9 mm/s (height unit: mm).

V^* \ H^*	0.3	0.6	0.9	1.2	1.5	1.8
0.4	+	×	×	×	×	×
0.8	+	0.5±0.02	0.75±0.01	0.77±0.01	0.77±0.01	0.77±0.01
1.2	+	+	0.75±0.01	0.95±0.04	0.95±0.03	▲
1.6	+	+	+	+	1.25±0.01	▲

As shown in Fig. 5 and Fig. 6, in addition to three previously described deposition status in the model (over-deposition, pressed-deposition and freeform-deposition), there were other two deposition statuses of tortuous filaments and discontinuous filaments. Tortuous filaments, discontinuous filaments and over-deposition would result in irregular width, height of DF and finally poor printing accuracy, which should be avoided. The non-perpendicularity of the nozzle to the substrate and the too large H^* resulted in the tortuous filaments. Ideally, if the nozzle was perfectly perpendicular to the substrate, tortuous filaments would not appear no matter how large H^* was. However, non-perpendicularity between the nozzle and the substrate could not be avoided due to installation errors and manufacturing errors. Thus, it was necessary to control H^* under a certain value to avoid tortuous filaments. Too fast nozzle velocity would result in discontinuous filaments. Thus, it was necessary to control V^* under a certain value to avoid discontinuous filaments. As shown in Fig. 5, the effectiveness of deposition statuses division of the model was verified as the analytical deposition statuses

division predicted the experimental statuses correctly except statuses of tortuous filaments and discontinuous filaments.

After verification of deposition statuses division of the proposed model, the model was used to select suitable H^* and V^* to make DF in pressed-deposition and freeform-deposition which had regular width and height. Prediction accuracy of the proposed model was verified by comparing the predicted analytical results and experimental results. The relative errors between analytical and experimental results were calculated using data from Table 4 to Table 9 and listed in Table 10 to Table 13. The maximum relative error of width and height between analytical and experimental results was 3.90%, verifying the prediction accuracy of the proposed model.

Meanwhile, the deposition statuses division and predicted width, height of DF under 2-levels of v_p were nearly same. Thus, piston velocity had little influence on the DF when H^* and V^* were controlled.

Table 10

Relative errors of analytical and experimental width results when v_e was set as 6 mm/s.

V^* \ H^*	0.3	0.6	0.9	1.2	1.5	1.8
0.4	+	×	×	×	×	×
0.8	+	2.91%	3.85%	3.90%	2.60%	2.60%
1.2	+	+	1.85%	3.19%	3.19%	3.19%
1.6	+	+	+	+	3.62%	▲

Table 11

Relative errors of analytical and experimental height results when v_e was set as 6 mm/s.

V^* \ H^*	0.3	0.6	0.9	1.2	1.5	1.8
0.4	+	×	×	×	×	×
0.8	+	0	0	3.90%	2.60%	2.60%
1.2	+	+	0	3.19%	3.19%	3.19%
1.6	+	+	+	+	0	▲

Table 12

Relative errors of analytical and experimental width results when v_e was set as 9 mm/s.

V^* \ H^*	0.3	0.6	0.9	1.2	1.5	1.8
0.4	+	×	×	×	×	×
0.8	+	3.88%	1.28%	0	0	0
1.2	+	+	1.85%	1.06%	1.06%	▲
1.6	+	+	+	+	2.17%	▲

Table 13

Relative errors of analytical and experimental height results when v_e was set as 9 mm/s.

V^* \ H^*	0.3	0.6	0.9	1.2	1.5	1.8

0.4	+	×	×	×	×	×
0.8	+	0	0	0	0	0
1.2	+	+	0	1.06%	1.06%	▲
1.6	+	+	+	+	0	▲

5. Conclusions

In this study, an analytical model is created to predict flow rate, width and height of DF for high viscosity material in piston-driven DIW. Next, Nivea Crème is selected as high viscosity material reference and experiments were conducted to verify the proposed model. The conclusions are drawn as follows:

(1) The ink extrusion process in time-domain included three stages due to the bulk modulus and yield stress of ink: 1) time delay and unstable flow at the at the starting time, 2) steady-state flow stage, 3) unstable flow at the end time. The flow rate in the steady-state flow stage could be calculated through mass conversation.

(2) Filaments deposition statuses were influenced by the dimensionless nozzle velocity V^* and the dimensionless height H^*. Piston velocity had little influence on deposition statuses, width and height of DF if V^* and H^* were determined.

(3) There were three deposition statuses which could be predicted using the analytical model: over-deposition, pressed-deposition, freeform-deposition. In addition to these three deposition statuses, additional two deposition statuses would appear in non-printable window: discontinuous filaments would appear when V^* was set too large and tortuous filaments would appear when H^* was set too large.

(4) The deposition statuses of over-deposition, discontinuous filaments and tortuous filaments should be avoided as they resulted in irregular width, height and low printing accuracy. The deposition statuses of pressed-deposition and freeform-deposition were controlled to get a high printing accuracy.

The proposed model has effectiveness and high prediction accuracy in modeling of flow rate, deposition statuses, width and height of deposited filament. This work will contribute to modeling and controlling the piston-driven DIW process for high viscosity materials. Current investigations are focused on the modeling of deposition filaments and future work will be conducted to model the printed layers and 3D parts to fully understand and control the piston-driven DIW process for high viscosity materials.

CRediT authorship contribution statement

Yongqiang Tu: Methodology, Writing-original draft. **Alaa Hassan**: Conceptualization, Methodology, Writing-review & editing. **Ali Siadat**: Supervision, Writing-review & editing. **Gongliu Yang**: Supervision, Writing-review & editing.

Declaration of Competing interest

The authors declare that they have no known competing financial interests or personal relationships that could have appeared to influence the work reported in this paper.

Acknowledgement

The authors would like to acknowledge the funding from the China Scholarship Council scholarship (No. 201906020135).

References

[1] A. I. Nurhudan, S. Supriadi, Y. Whulanza, and A. S. Saragih, "Additive manufacturing of metallic based on extrusion process: A review," *Journal of Manufacturing Processes,* vol. 66, pp. 228-237, 2021/06/01/ 2021.

[2] L. Palmeira Belotti, J. A. W. van Dommelen, M. G. D. Geers, C. Goulas, W. Ya, and J. P. M. Hoefnagels, "Microstructural characterisation of thick-walled wire arc additively manufactured stainless steel," *Journal of Materials Processing Technology,* vol. 299, p. 117373, 2022/01/01/ 2022.

[3] I. Astm, "ASTM52900-15 standard terminology for additive manufacturing—general principles—terminology," *ASTM International, West Conshohocken, PA,* vol. 3, no. 4, p. 5, 2015.

[4] S. Tarassoli, Z. Jessop, A. Al-Sabah, I. Simoes, and I. Whitaker, "Searching for the optimal bioink in extrusion-based 3D bioprinting for reconstructive surgery," *International Journal of Surgery,* vol. 55, p. S95, 2018/07/01/ 2018.

[5] Z. M. Jessop *et al.*, "Printability of pulp derived crystal, fibril and blend nanocellulose-alginate bioinks for extrusion 3D bioprinting," *Biofabrication,* vol. 11, no. 4, p. 045006, 2019/07/08 2019.

[6] X. B. Chen and K. Jun, "Modeling of positive-displacement fluid dispensing processes," *IEEE Transactions on Electronics Packaging Manufacturing,* vol. 27, no. 3, pp. 157-163, 2004.

[7] P. T. Smith, A. Basu, A. Saha, and A. Nelson, "Chemical modification and printability of shear-thinning hydrogel inks for direct-write 3D printing," *Polymer,* vol. 152, pp. 42-50, 2018/09/12/ 2018.

[8] R. Tu and H. A. Sodano, "Additive manufacturing of high-performance vinyl ester resin via direct ink writing with UV-thermal dual curing," *Additive Manufacturing,* vol. 46, p. 102180, 2021/10/01/ 2021.

[9] J. Hinton Thomas *et al.*, "Three-dimensional printing of complex biological structures by freeform reversible embedding of suspended hydrogels," *Science Advances,* vol. 1, no. 9, p. e1500758.

[10] F. Zhu *et al.*, "3D Printing of Ultratough Polyion Complex Hydrogels," *ACS Applied Materials & Interfaces,* vol. 8, no. 45, pp. 31304-31310, 2016/11/16 2016.

[11] L. Sun, S. T. Parker, D. Syoji, X. Wang, J. A. Lewis, and D. L. Kaplan, "Direct-write assembly of 3D silk/hydroxyapatite scaffolds for bone co-cultures," (in eng), *Advanced healthcare materials,* vol. 1, no. 6, pp. 729-735, 2012.

[12] M. Kim and J.-W. Choi, "Rubber ink formulations with high solid content for direct-ink write process," *Additive Manufacturing,* vol. 44, p. 102023, 2021/08/01/ 2021.

[13] K. Sun, T.-S. Wei, B. Y. Ahn, J. Y. Seo, S. J. Dillon, and J. A. Lewis, "3D Printing of Interdigitated Li-Ion Microbattery Architectures," *Advanced Materials,*

https://doi.org/10.1002/adma.201301036 vol. 25, no. 33, pp. 4539-4543, 2013/09/06 2013.

[14] M. Wehner *et al.*, "An integrated design and fabrication strategy for entirely soft, autonomous robots," *Nature,* vol. 536, no. 7617, pp. 451-455, 2016/08/01 2016.

[15] A. Frutiger *et al.*, "Capacitive Soft Strain Sensors via Multicore–Shell Fiber Printing," *Advanced Materials,* https://doi.org/10.1002/adma.201500072 vol. 27, no. 15, pp. 2440-2446, 2015/04/01 2015.

[16] M. Vlasea and E. Toyserkani, "Experimental characterization and numerical modeling of a micro-syringe deposition system for dispensing sacrificial photopolymers on particulate ceramic substrates," *Journal of Materials Processing Technology,* vol. 213, no. 11, pp. 1970-1977, 2013/11/01/ 2013.

[17] J. M. Lee and W. Y. Yeong, "A preliminary model of time-pressure dispensing system for bioprinting based on printing and material parameters," *Virtual and Physical Prototyping,* vol. 10, no. 1, pp. 3-8, 2015/01/02 2015.

[18] R. Suntornnond, E. Y. S. Tan, J. An, and C. K. Chua, "A Mathematical Model on the Resolution of Extrusion Bioprinting for the Development of New Bioinks," (in eng), *Materials (Basel),* vol. 9, no. 9, p. 756, 2016.

[19] N. Haghbin, D. Bone, and K. Young, "Controlled extrusion-based 3D printing of micro-channels with the geometric modelling of deposited roads," *Journal of Manufacturing Processes,* vol. 67, pp. 406-417, 2021/07/01/ 2021.

[20] M. Athanasiadis, A. Pak, D. Afanasenkau, and I. R. Minev, "Direct Writing of Elastic Fibers with Optical, Electrical, and Microfluidic Functionality," *Advanced Materials Technologies,* https://doi.org/10.1002/admt.201800659 vol. 4, no. 7, p. 1800659, 2019/07/01 2019.

[21] G. Percoco, L. Arleo, G. Stano, and F. Bottiglione, "Analytical model to predict the extrusion force as a function of the layer height, in extrusion based 3D printing," *Additive Manufacturing,* vol. 38, p. 101791, 2021/02/01/ 2021.

[22] X. B. Chen, G. Shoenau, and W. J. Zhang, "Modeling of time-pressure fluid dispensing processes," *IEEE Transactions on Electronics Packaging Manufacturing,* vol. 23, no. 4, pp. 300-305, 2000.

[23] L. del-Mazo-Barbara and M.-P. Ginebra, "Rheological characterisation of ceramic inks for 3D direct ink writing: a review," *Journal of the European Ceramic Society,* 2021/08/18/ 2021.

[24] R. Plachy, C. Hellmich, F. Arthofer, S. Robin, A. Holzner, and S. Scheiner, "Hydrostatic compression tests, capillary rheometry tests, and extrusion tests performed on unvulcanized rubber confirm importance of compressibility for die swell — Arguments from dimensional analysis," *Polymer Testing,* vol. 101, p. 107289, 2021/09/01/ 2021.

[25] N. Valipour Motlagh and M. Taghipour-Gorjikolaie, "Fuzzy based models for estimating static contact angle and sliding angle of liquid drops," *Progress in Organic Coatings,* vol. 119, pp. 183-193, 2018/06/01/ 2018.

[26] H. Yuk and X. Zhao, "A New 3D Printing Strategy by Harnessing Deformation, Instability, and Fracture of Viscoelastic Inks," *Advanced Materials,* https://doi.org/10.1002/adma.201704028 vol. 30, no. 6, p. 1704028, 2018/02/01 2018.

[27] N. Paxton, W. Smolan, T. Böck, F. Melchels, J. Groll, and T. Jungst, "Proposal to assess printability of bioinks for extrusion-based bioprinting and evaluation of rheological

properties governing bioprintability," *Biofabrication,* vol. 9, no. 4, p. 044107, 2017/11/14 2017.

[28] Y. Tu, J. A. Arrieta-Escobar, A. Hassan, U. K. u. Zaman, A. Siadat, and G. Yang, "Optimizing Process Parameters of Direct Ink Writing for Dimensional Accuracy of Printed Layers," *3D Printing and Additive Manufacturing,* 2021.